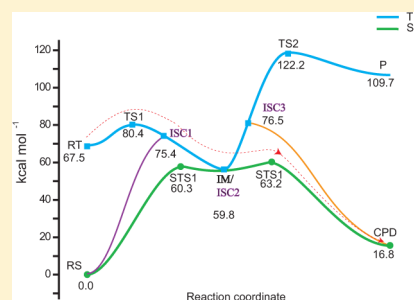


# Physical Quenching in Competition with the Formation of Cyclobutane Pyrimidine Dimers in DNA Photolesion

Hongmei Zhao, Kunhui Liu, Di Song, and Hongmei Su\*

Beijing National Laboratory for Molecular Sciences (BNLMS), State Key Laboratory of Molecular Reaction Dynamics, Institute of Chemistry, Chinese Academy of Sciences, Beijing 100190, P. R. China

**ABSTRACT:** The potential energy profiles toward formation of cyclobutane pyrimidine dimers CPD and the physical quenching after UV excitation were explored for the dinucleotide thymine dinucleoside monophosphate (TpT) using density functional theory ( $\omega$ B97XD) and the time-dependent density functional theory (TD- $\omega$ B97XD). The  $\omega$ B97XD functional that includes empirical dispersion correction is shown to be an appropriate method to obtain rational results for the current large reaction system of TpT. Photophysical quenching is shown to be predominant over the photochemical CPD formation. Following the initial excitation to the  $^1\pi\pi^*$  state, the underlying dark  $^1n\pi^*$  state bifurcates the excited population to the prevailing IC to  $S_0$  and the small ISC to the long-lived triplet state  $T_1$  via  $T_4$  ( $^3\pi\pi^*$ ) state that has negligible energy gap with  $^1n\pi^*$  state. Even for the reactive  $T_1$  state, two physical quenching pathways resulting in the conversion back to ground-state reactant via the  $T_1/S_0$  crossing points are newly located, which are in strong competition with CPD formation. These results provide rationale for the recently observed nanosecond triplet decay rates in the single-stranded (dT)<sub>18</sub> and inefficiency of deleterious CPD formation, which allow for a deeper understanding of DNA photostability.



## INTRODUCTION

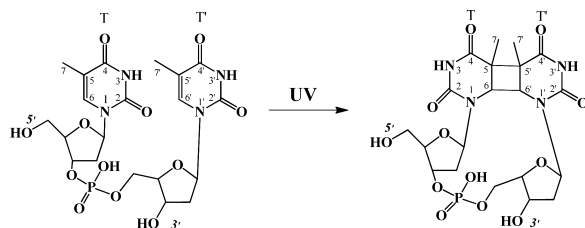
Absorption of UV radiation by nucleic acid bases, the most important UV chromophores of nucleic acids, is a process of primary biophysical and biochemical interest. The accumulation of photolesions leads to genetic modifications and ultimately to diseases like skin cancer. The photostability of DNA bases is thus fundamental for the life sustainability. UV-induced photochemical damage has been observed for the monomers, oligonucleotides, and DNA.<sup>1–4</sup> The most abundant lesion is the formation of cyclobutane pyrimidine dimers (CPDs) (Scheme 1),<sup>3,4</sup> in which the adduct is formed via a [2 + 2] photocycloaddition involving the C=C double bonds of the adjacent pyrimidines. In principle, the excited singlet and triplet states of the pyrimidine play a critical role in CPD lesion.

Significant advances in understanding the excited singlet-state photophysics of the nucleic acid bases have been made in

recent years. Kohler and co-workers<sup>5</sup> observed that UV irradiation of the single-stranded (dT)<sub>18</sub> leads to the dimerization of cis-syn thymine in less than 1 ps. The ultrafast process of CPD formation indicated that the dimerization occurs directly from the singlet  $^1\pi\pi^*$  state. Theoretically, CASSCF and CASPT2 calculations<sup>6,7</sup> on two stacked thymines and PCM/TD-M052X calculations on the dinucleotide TpT<sup>8</sup> indicated that the concerted [2 + 2] dimerization takes place on a singlet excited state and proceeds along a barrierless path to form CPD on the ground state through an  $S_0/S_1$  conical intersection (CI). Furthermore, the structure cannot change much in the picosecond time scale and the calculated conformation of CI is further away from stacked thymine configuration in B-DNA. Therefore, the dimerization occurs only for the two neighboring thymine residues that are already at a configuration near the CI structure, which is infrequent in the DNA strands. The highly conformation restriction explains the very low quantum yield ( $\sim 3\%$ ) of CPD.<sup>9</sup>

It has also been proposed that the long-lived triplet states play key roles in the CPD formation.<sup>10</sup> The structure of single-stranded DNA is mobile,<sup>11</sup> and the frequent conformation change makes the triplet state possible to encounter thymine residue with suitable conformation within its long lifetime, leading to CPD. The triplet CPD formation mechanism has

**Scheme 1. Formation of Cyclobutane Pyrimidine Dimers (CPDs) upon UV Irradiation of DNA (Demonstrated with the Dinucleotide TpT)<sup>a</sup>**



<sup>a</sup>The atomic numbering used hereafter is also labeled.

**Special Issue:** International Conference on Theoretical and High Performance Computational Chemistry Symposium

**Received:** February 28, 2014

**Revised:** June 24, 2014

**Published:** June 25, 2014

been confirmed by the triplet photosensitization experiments.<sup>12–17</sup> The reactivity of the triplet state toward CPD formation has also gained support from the theoretical calculation,<sup>18</sup> where the hybrid DFT calculation has been employed to investigate the triplet pathway for dimerization of two single-stacked thymines to form CPD.

Recently, Banyasz et al.<sup>8</sup> measured the excitation wavelength dependence of the intersystem crossing quantum yield  $\phi_{\text{ISC}}$  for the thymidine monophosphate (TMP). It was observed that  $\phi_{\text{ISC}}$  displayed a strong wavelength dependence, which was in contrast with the constant CPD quantum yield of  $\phi_{\text{CPD}}$  for (dT)<sub>20</sub>. On the basis of this observation, it was speculated that the contribution of triplet  $^3\pi\pi^*$  states to CPD formation should be lower than 10% if taking into account the experimental errors. Compared to the measured large T<sub>1</sub> quenching rate constants ( $\sim 10^{10} \text{ M}^{-1} \text{ s}^{-1}$ ),<sup>10</sup> the inefficiency in formation of CPD photoproducts through the triplet route indicates competitive physical quenching processes may exist, resulting in very small product yields eventually. Interestingly, a triplet biradical intermediate was located by CASPT2 calculations, which can be used to rationalize the quenching of thymine triplet excitations.<sup>19</sup> A barrierless path from two stacked thymines in the triplet state to the biradical intermediate was revealed, which should correspond to a femtosecond or picosecond lifetime for the triplet decay. However, the most recent time-resolved IR spectroscopy experiments observed that triplet decay in (dT)<sub>18</sub> or the locked dinucleotide T<sub>1</sub>LPT<sub>L</sub> follows nanosecond rates.<sup>20</sup> By spectral analysis, two time constants were derived and ascribed to the decay of the local thymine triplet state (with a  $\sim 10$  ns time constant) via the biradical intermediate (lifetime  $\sim 60$  ns). The spectroscopic evidence was thus first acquired for the generally assumed triplet biradical intermediate.<sup>20</sup> The observed nanosecond rates for the triplet decay are in conflict with the theoretically expected femtosecond or picosecond lifetime along a barrierless path. Therefore, further studies are required to clarify the triplet quenching mechanism and rationalize the recent experimental results.

The present work mainly focuses on examining the important physical quenching processes in competition with the photochemical CPD formation theoretically. The dinucleotide TpT, the smallest DNA fragment sustaining the constraints of the DNA backbone, is chosen to be the reaction system, just as in the most photoreaction experiment. The interaction of excited singlet, triplet states, and ground state is explored by DFT and TD-DFT calculations with the  $\omega$ B97XD<sup>21</sup> functional including solvent effects.  $\omega$ B97XD is a recently developed long-range corrected functional that includes empirical dispersion correction. With this method, the detailed nonradiative deactivation pathways are revealed, showing how singlet excited state evolves to triplet and ground singlet states. Two physical quenching pathways competing with CPD formation along the triplet state are located, which takes place through the T<sub>1</sub>/S<sub>0</sub> surface crossings along the dimerization coordinate. These results allow for a deeper understanding of the inefficiency CPD formation through triplet route and shed further light on DNA photostability.

## THEORETICAL METHODS

In the present work, we choose the smallest DNA fragment, the dinucleotide thymine dinucleoside monophosphate (TpT), as the reaction system, which is close to the natural situation of DNA strand. Our analyses were performed by using a recently

developed long-range corrected functional,  $\omega$ B97XD,<sup>21</sup> from Head-Gordon and co-workers that includes empirical dispersion correction. The treatment with dispersion interactions can improve descriptions for stacked DNA systems.<sup>22</sup> The first excited singlet electronic state (S<sub>1</sub>) geometries of TpT were optimized and the excitation energies were calculated with time-dependent density functional theory (TD- $\omega$ B97XD). The geometries of the reactants, products, intermediates, and transition states along the T<sub>1</sub> or S<sub>0</sub> state were calculated using  $\omega$ B97XD functional with 6-311G(d,p) basis set. The stationary points of the reactant, intermediates, and products was identified as local minima by harmonic frequency analysis. The transition states are identified as the first-order saddle point. The intrinsic reaction coordinate (IRC)<sup>23</sup> calculations are carried out to confirm that the transition states connect the right minima. The single-point energies were calculated at the  $\omega$ B97XD/6-311++G(d,p) level with the  $\omega$ B97XD/6-311G(d,p) optimized geometries. As all DNA damage processes are supposed to take place in aqueous solution, bulk solvation effects were simulated on the basis of the optimized geometries obtained in the gas phase by using the polarized continuum model (PCM) at the same level.<sup>24</sup> Bulk solvation with the dielectric constant  $\epsilon = 4.3$  is used to simulate the apolar surroundings in DNA.<sup>25</sup> The B3LYP<sup>26,27</sup> calculations were performed in parallel at the same level to compare with the  $\omega$ B97XD results. The calculations were carried out using the Gaussian 09 program package.<sup>28</sup>

## RESULTS AND DISCUSSIONS

**Validation of Computational Approach.** It had been reported that the density functional theory with dispersion method can substantially improve the theoretical description of the formation of the intrastrand photolesions product, compared to pure or hybrid GGA functionals.<sup>22</sup> Therefore, the long-range corrected functional,  $\omega$ B97XD, from Head-Gordon and co-workers that includes empirical London dispersion was used in the calculations of this work.

The cyclobutane pyrimidine dimers (CPDs) are major mutagenic photoproducts formed upon absorption of UV irradiation. The excited singlet and triplet states are involved and play key roles in the CPD formation reaction. To verify if the  $\omega$ B97XD method can provide the correct description of the excited states and is suitable to investigate the photoreaction mechanism, we performed several single-point test calculations to compare with the reported CASPT2/CASSCF results. Table 1 shows the vertical excitation energies calculated for a gas-phase model of two stacked thymines (TT pair) in its ideal B-DNA conformation or for the isolated thymine base, from the ground state to different excited states.

**Table 1. Computed Vertical Excitation Energies (eV) of the Excited Singlet and Triplet States with Different Methods**

	CASPT2/ CASSCF	TD- $\omega$ B97XD	TD- M052X	TD- B3LYP
TT <sup>a</sup> -S <sub>1</sub>	5.12 <sup>b</sup>	4.98	4.90	4.59
thymine-S <sub>1</sub>	5.41 <sup>c</sup>	5.14	5.04	4.76
thymine-T <sub>1</sub>	3.59 <sup>c</sup>	3.41	3.54	3.34
thymine-T <sub>2</sub>	4.75 <sup>c</sup>	4.68	4.59	4.34
thymine-T <sub>3</sub>	5.14 <sup>c</sup>	5.06	5.75	4.75

<sup>a</sup>Stacked TT in the ideal B-DNA conformation. <sup>b</sup>See ref 7, CASPT2/CASSCF(12,12)/6-31G\*. <sup>c</sup>See ref 29, CASSCF(14,10).

For TT pair, the CASPT2/CASSCF(12,12)/6-31G\* calculated  $S_0$ – $S_1$  excitation energy is 5.12 eV.<sup>7</sup> It can be seen from Table 1 that our TD- $\omega$ B97XD/6-311G(d,p) calculation result of 4.98 eV is in good agreement with the CASPT2 result. Similarly, for the isolated thymine, the  $S_0$ – $S_1$  excitation energy of 5.14 eV obtained here is also in agreement with the CASSCF(14,10)/ANO-S result of 5.41 eV.<sup>29</sup> In addition, the excitation energies of the lowest three excited triplet states (3.41, 4.68, and 5.06) at the TD- $\omega$ B97XD/6-311G(d,p) level obtained here are also very close to that of CASPT2//CASSCF(14,10) calculations (3.59, 4.75, and 5.14).<sup>29</sup> These test computation results indicate that TD- $\omega$ B97XD offers an alternative approach and can obtain excited-state results in agreement with CASPT2 and CASSCF.

We also tested other time-dependent density functional theory methods of TD-M052X and TD-B3LYP, which was used to investigate the cyclobutane dimmers (CPD) formation reaction.<sup>8,18</sup> The results are also listed in Table 1. Compared with TD-M052X calculation results, the excitation energies of TT- $S_1$ , thymine- $S_1$ ,  $T_2$ , and  $T_3$  obtained using the TD- $\omega$ B97XD method are closer to CASSCF and CASPT2 results, whereas the excitation energies using TD-B3LYP method are all underestimated. It shows here that more accurate results can be obtained with the TD- $\omega$ B97XD method, compared to the methods of TD-M052X and TD-B3LYP.

In the following section, we chose  $\omega$ B97XD and TD- $\omega$ B97XD to investigate the UV-induced reaction of CPD formation in the ground state and the excited triplet and singlet state. The potential energy profiles along  $S_0$  and  $T_1$  states were first calculated. The optimized structures of reactants, intermediates, transition states, and products are shown in Figure 1. The computed energies in vacuum and solution are listed in Table 2. It can be seen that the larger basis set 6-311++G(d,p) offers slight improvement for the stationary point energies and barrier height. We use the energies calculated with the 6-311G(d,p) basis set for the discussion. The zero-point energy (ZPE) corrections affect the relative energies slightly and thus are not taken into account in the following discussion.

**Potential Energy Profile on the  $S_0$  Surface.** For the  $S_0$  state, the transition states of consecutive reaction (STS1, STS2) and the concerted reaction (STS3) are both located, as shown in Figure 2. The first transition state STS1 connects the reactant RS with the intermediate biradical minimum SIM with a barrier height of 60.3 kcal mol<sup>-1</sup>. The transition vector of STS1 corresponds to the C6–C6' bond stretching. In SIM, the C6 atom is bonded with C6' atom with the bond length of C6–C6' 1.623 Å, and the distance between C5 and C5' atom is 3.091 Å. According to spin density analysis, the spin densities on C5 and C5' are +0.84 and –0.83 respectively, indicating the localization of the unpaired electron densities on the C5 and C5'. This confirms the biradical feature of the singlet biradical complex SIM. Then the highly reactive biradical structure forms CPD easily, via a low barrier of 4.4 kcal mol<sup>-1</sup> (STS2). The consecutive pathway faces a rate-limiting barrier height of 63.2 kcal mol<sup>-1</sup> and thus is energetically inaccessible.

Additionally, the cycloaddition reaction of TpT on the  $S_0$  surface could also be a concerted process through one four-membered cyclic transition state STS3 (Figures 1 and 2). In STS3, the double bonds of C5–C6 and C5'–C6' are stretched, and the cross-linking occurs between C5 and C5' and between C6 and C6'. All bond breaking and bond making occurs in a single step, yielding the final CPD product via STS3

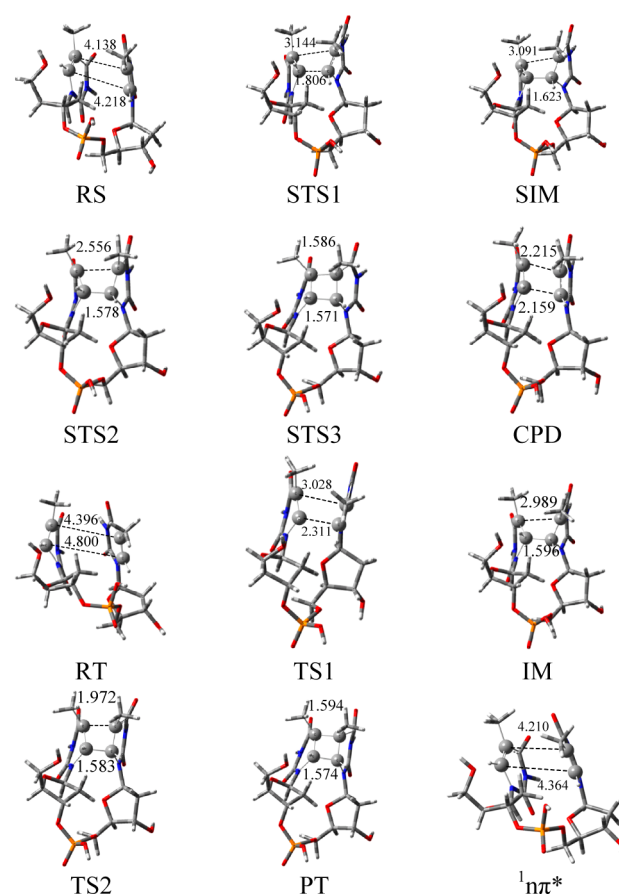


**Figure 1.** Optimized geometries of reactants, intermediates, transition states, and products in the  $S_0$ ,  $T_1$ , and  $S_1$  states at the  $\omega$ B97XD/6-311G(d,p) level. Optimized geometry for the singlet excited state  $S_1$  at the TD- $\omega$ B97XD/6-311G(d,p) level. Bond lengths are in angstroms.

**Table 2.** Relative Energies (without ZPE Correction), kcal mol<sup>-1</sup>, of the Stationary Structures along the  $T_1$  and  $S_0$  Reaction Pathways, Obtained from  $\omega$ B97XD Calculations

	$\omega$ B97XD/6-311G(d,p)		$\omega$ B97XD/6-311++G(d,p)	
	vacuum		vacuum	$\epsilon = 4.3$
RS	0		0	0
STS1	60.3		61.9	60.0
SIM	58.8		57.7	56.2
STS2	63.2		65.8	64.0
STS3	94.1		91.9	89.5
CPD	16.8		16.7	15.6
RT	67.5		68.0	68.6
TS1	80.4		78.7	78.0
IM	59.8		58.7	57.2
TS2	122.2		121.9	119.9
P	109.7		109.9	109.4

overcoming a barrier of 90.0 kcal mol<sup>-1</sup>, much higher than STS2.

The influence of solvation is also considered. As shown in Table 2, the barrier heights decrease in the consecutive and the concerted reaction steps to 64.0 and 89.5 kcal mol<sup>-1</sup>, respectively, compared to the corresponding vacuum values of 65.8 and 91.9 kcal mol<sup>-1</sup>. So the bulk solvation only slightly influences the barrier height. Whether through consecutive or concerted pathway, the potential energy profiles clearly show

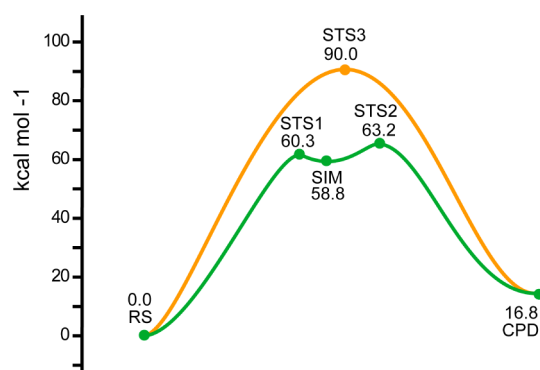


**Figure 2.** Potential energy profiles on the  $S_0$  surface for the formation of CPD. The relative energies are obtained from the  $\omega$ B97XD/6-311g(d,p) calculation and indicated in kcal mol $^{-1}$ .

that the CPD formation on the ground state is energetically inaccessible at room temperature.

**Potential Energy Profile on the  $T_1$  Surface.** Starting from the triplet reactant  $T_pT$  (denoted as RT), a consecutive reaction channel is revealed in the triplet state and the potential energy profile is presented in Figure 3. Due to the  $C=C \pi \rightarrow$

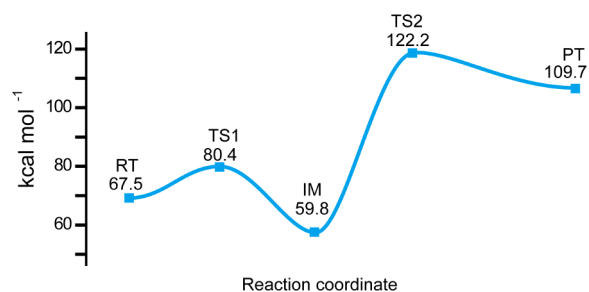


**Figure 3.** Potential energy profiles on the  $T_1$  surface for the formation of CPD. The relative energies are obtained from the  $\omega$ B97XD/6-311g(d,p) calculation and indicated in kcal mol $^{-1}$ .

$\pi^*$  excitation, the C5–C6 bond of RT becomes a  $\sigma$ -bond (1.489 Å). The triplet RT is a biradical with the spin densities localized on C5 and C6 atoms. Thus, the C5 and C6 atoms of one thymine residues are reactive and could be bonded with C5' and C6' atoms of the other thymine residues stepwisely to form CPD dimer.

The first step proceeds through initial attack of C6 on C6' facily with a low barrier of 12.9 kcal mol $^{-1}$ , leading to the intermediate IM which lies 7.7 kcal mol $^{-1}$  below the triplet reactant RT. It can be seen from Table 2 that the bulk solvation affects slightly the barrier (9.4 kcal mol $^{-1}$ ). In the intermediate IM, the C6 atom bonds with C6' atom and the spin densities are localized on C5 and C5' atoms. So IM is of a biradical nature. Taking into account the bulk solvation effect, the exothermicity of IM is increased to 11.4 kcal mol $^{-1}$  (Table 2). Due to the low barrier, the first step can take place favorably on the triplet state. However, the consecutive step of the C5–C5' cross-link from IM to TS2 overcomes a high energy barrier of 62.4 kcal mol $^{-1}$ , forming the triplet cyclobutane pyrimidine dimmer CPD (denoted as P). The triplet CPD product is quite unstable and has a relative energy of 109.7 kcal mol $^{-1}$  with respect to the singlet reactant RS zero level. Thus, there is little possibility that the CPD forms solely in the triplet state.

**Comparison of  $\omega$ B97XD and B3LYP Calculated Results.** We also performed the calculation with the most

popular functional Becke three-parameter hybrid B3LYP density functional,<sup>26,27</sup> to compare with the results of Head-Gordon's  $\omega$ B97XD functional<sup>21</sup> at the same level. The B3LYP energies of the stationary structures in the gas phase and solution are collected in Table 3. For the consecutive pathway

**Table 3.** Relative Energies (without ZPE Correction), kcal mol $^{-1}$ , of the Stationary Structures along the  $T_1$  and  $S_0$  Reaction Pathways, Obtained from B3LYP Calculations

	B3LYP/6-311G(d,p)		B3LYP/6-311++G(d,p)	
	vacuum		vacuum	$\epsilon = 4.3$
RS	0		0	0
STS2	72.3		70.7	68.9
STS3	96.3		93.1	91.1
CPD	31.5		31.3	30.1
RT	67.8		67.4	68.0
TS1	81.4		79.2	78.2
IM	69.4		68.2	66.8
TS2	127.7		126.9	125.3
P	121.4		121.5	120.9

in the  $S_0$  state, only one transition state STS2 with a barrier of 72.3 kcal mol $^{-1}$  was located. The IRC calculation in the region between the STS2 and RS did not converge to any intermediate; that is, STS1 and SIM were not located by B3LYP calculations.

The calculated results here with  $\omega$ B97XD or B3LYP are compared with higher level calculations. In the CASSCF and CASPT2 calculations performed for two stacked thymines,<sup>6</sup> two transition states (STS1, STS2) with the barrier of 61.0 and 63.1 kcal mol $^{-1}$  and a singlet biradical intermediate SIM (59.8 kcal mol $^{-1}$ ) were located along the ground-state consecutive reaction pathway. As shown in Figure 2, similar results can be obtained by our  $\omega$ B97XD calculations, and the  $\omega$ B97XD/6-311G(d,p) energies (60.3, 63.2, 58.8, and 16.8 kcal mol $^{-1}$  for STS1, STS2, SIM, and CPD) are in nice agreement with those obtained by CASSCF and CASPT2 calculations (61.0, 63.1, 59.8, and 19.0 kcal mol $^{-1}$  for STS1, STS2, SIM, and CPD).<sup>6</sup> However, the B3LYP calculation can only locate one transition state STS2 and the energies (72.3 and 31.5 kcal mol $^{-1}$  for STS2 and CPD) deviate largely from the higher level CASSCF/CASPT2 results. It shows here that  $\omega$ B97XD functional provide a better approach than B3LYP in calculating the reaction process and energies.

As for the triplet-state pathways, it can be seen from Tables 2 and 3 that the energy barriers of TS1 and TS2 are decreased by 1.0 and 5.1 kcal mol $^{-1}$  using  $\omega$ B97XD functional, and the energies of IM and P of  $\omega$ B97XD results are decreased by 9.6 and 11.7 kcal mol $^{-1}$ , compared with those obtained from B3LYP functional. Previous studies indicated that the DFT description of intrastrand cross-link formation can be improved by inclusion of London dispersion correction,<sup>22</sup> because inclusion of dispersion can improve the structural description of di- or trinucleotides by maintaining their  $\pi$ -stacked mode. Different from B3LYP, the  $\omega$ B97XD functional includes empirical London dispersion correction. Also due to other parametrization, different results are obtained from these two DFT functionals.

Overall, it can be seen from the potential energy profiles on the  $T_1$  and  $S_0$  surface that the CPD formation process solely along the triplet or singlet ground state exhibit high barriers and is thus energetically inaccessible at room temperature. Possibly,

surface interactions between the singlet states and triplet state may exist, which are crucial for understanding the CPD formation mechanism.

**ISC from the Singlet Excited State to the Triplet Excited State.** The first singlet excited state of TpT is optimized in a vacuum at the TD- $\omega$ B97XD/6-311G(d,p) level of theory, and its equilibrium geometry is shown in Figure 1. Comparing the ground-state and excited-state geometries, one of the C=O bond of TpT is stretched from 1.216 to 1.328 Å. Frontier molecular orbital analysis also indicates the  $n\pi^*$  character for the first singlet excited state. At the equilibrium geometry of  $^1n\pi^*$ , the energies of triplet states of  $T_4$ ,  $T_3$ ,  $T_2$ , and  $T_1$  are calculated, and the results are shown in Figure 4. It

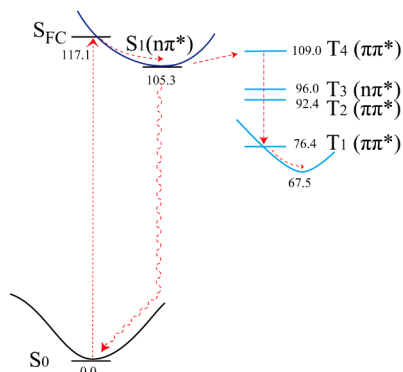


**Figure 4.** TD- $\omega$ B97XD/6-311G(d,p) calculated excitation energies ( $\text{kcal mol}^{-1}$ ) for TpT, and schematic excited-state relaxation pathways denoted with red dotted lines.

can be seen that the energy of  $T_4$  is in close proximity with the  $^1n\pi^*$  state. In addition, our calculations show that the character of the lowest four excited triplet states is  $\pi\pi^*$  for  $T_1$ ,  $T_2$ , and  $T_4$  and  $n\pi^*$  for  $T_3$ . Considering the classical propensity rule (the EI-Sayed rule),<sup>30</sup> ISC from  $^1n\pi^*$  state to an excited triplet state requires the excited triplet state to be a state with substantial  $\pi\pi^*$  character to mediate the correlated spin-orbital coupling.  $T_4$  state has  $\pi\pi^*$  character and the energy gap between the  $S_1$  and  $T_4$  state is  $3.8 \text{ kcal mol}^{-1}$  ( $0.16 \text{ eV}$ ). The close degeneracy between the states of different multiplicity can compensate for very small spin-orbit coupling<sup>31–34</sup> and drive efficient ISC. Due to near-degeneracy between singlet excited state  $^1n\pi^*$  and triplet excited state  $T_4$ , the ISC takes place from  $S_1$  to the receiver  $T_4$  state. Subsequently,  $T_4$  undergoes fast IC to the lowest  $T_1$  ( $^3\pi\pi^*$ ) state, where CPD reaction occurs. These results indicate that the dark  $^1n\pi^*$  state can serve as a doorway state, resulting in excited-state depopulation from singlet manifold to triplet manifold.

It should be noted that intersystem crossing to triplet manifold only accounts for a small fraction in the excited-state relaxation. For isolated thymine,<sup>35–37</sup> it had been found that the conical intersection (CI) between the singlet excited- $^1n\pi^*$ -state and ground-state results in the ultrafast internal conversion, which is the dominant process, and a small fraction of the  $S_1(n\pi^*)$  population undergoes intersystem crossing to the lowest triplet state  $T_1(\pi\pi^*)$ . For stacked thymines (TT pair), CASSCF and CASPT2 calculations<sup>6</sup> revealed a barrierless relaxation process from Franck–Condon region to the  $S_0/S_1$  conical intersection. Minimum energy path calculations suggested that  $S_0/S_1$  CI can either evolve to the product or revert back to the original reactant. So the CPD formation can directly occur via  $S_1$  state. Similarly, the  $S_0/S_1$  CI were also

located by PCM/TD-M052x/6-31G(d) calculations<sup>8</sup> for the dinucleotide TpT, with a representative structure reported (the C5–C5' and C6–C6' distances are 2.5 and 2.06 Å, respectively). By performing TD- $\omega$ B97XD/6-311G(d,p) calculations, we also found a similar structure (the C5–C5' distance of 2.52 Å and the C6–C6' distance of 1.98 Å), and the calculated energy gap between  $S_1$  and  $S_0$  at this point is only 0.34 eV, confirming further the existence of  $S_0/S_1$  CI. Altogether, these results indicate that the singlet excited state  $^1n\pi^*$  governs the excited-state depopulation. The excited-state relaxation channels are prevailed by internal conversion (IC) to  $S_0$ , which is accompanied by the small intersystem crossing (ISC) to the long-lived triplet state  $T_1$ . Although the quantum yield is low, the long-lived triplet state is believed to be a possible reactive intermediate leading to the CPD photo-product.

### Nonadiabatic Photochemical and Photophysical Pathways from the Triplet to Singlet Ground State.

Although the formation of CPD solely in the triplet or singlet ground state is energetically inaccessible due to the high barriers, the  $T_1/S_0$  surface crossing can facilitate the reaction process substantially. To obtain the singlet–triplet interaction profile, we performed IRC calculations at the  $\omega$ B97XD/6-311G(d,p) level using the mass-weighted internal coordinate with the small step size of  $0.01 \text{ amu}^{1/2} \text{ bohr}$  and obtained the minimum energy path for triplet. For each point along the triplet minimum energy path, the single-point energy is calculated in the singlet state, from which the  $T_1/S_0$  surface crossing points are obtained. As shown in Figure 5, three  $T_1/S_0$

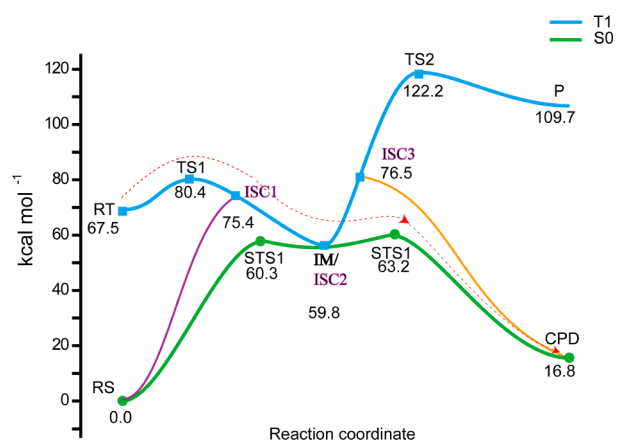


**Figure 5.** Potential energy profiles for the CPD formation along either the  $T_1$  (blue solid lines) or  $S_0$  (green solid lines) state and the interaction between the two states, obtained from  $\omega$ B97XD/6-311G(d,p) calculations. The relative energies are indicated in  $\text{kcal mol}^{-1}$ . The red dotted lines highlight the energetically most feasible pathway leading to CPD formation. The purple and orange solid lines denote the minimum energy paths for the decay of ISC1 or ISC3 in the ground state.

crossing points ISC1, ISC2, and ISC3 have been located. After obtaining these crossing points, minimum energy path calculations are performed further to locate their decay pathways in the ground state.

As shown in Figure 5, the second crossing point ISC2 is a stationary point identical with the triplet biradical intermediate IM. With two unpaired electrons distributed to different sets of atoms C5 and C5', the biradical IM in its triplet and singlet state is degenerate in energy. For ISC2, a similar structure in

two stacked thymines (TT pair) was located by CASPT2 calculations,<sup>19</sup> where the minimum energy path starting from the locally excited triplet state (RT) showed a barrierless path toward the biradical intermediate at ISC2. For such a barrierless path, a femto- or picosecond time constant for the triplet decay would be expected. But a most recent experimental study observed different results. By time-resolved IR spectroscopy measurements,<sup>20</sup> it was observed that the triplet decay in (dT)<sub>18</sub> or the locked dinucleotide T<sub>1</sub>P<sub>1</sub>T<sub>1</sub> followed nanosecond rates, and two time constants for the kinetic processes were determined,<sup>20</sup> corresponding respectively to the decay from the local thymine triplet state to the biradical intermediate (with a ~10 ns time constant) and the decay of the biradical intermediate to ground-state reactant (lifetime ~60 ns). The experimental time constants were compared with the CASPT2 results, and it was stated that the theoretically predicted barrierless path should correspond to a femtosecond or picosecond time constant, in conflict with the observed nanosecond rates for the triplet decay.<sup>20</sup>

Our calculation may provide new insights to rationalize these recent experimental results. As shown in Figure 5, the  $\omega$ B97XD/6-311G(d,p) calculations reveal that the decay of the locally excited triplet state (RT) to the biradical intermediate at ISC2 is not barrierless. It requires us to surmount a barrier of 12.9 kcal mol<sup>-1</sup> via TS1. With such an energy barrier, the triplet decay to form the biradical intermediate is expected to take place with a much slower rate, compared to ultrafast barrierless process, matching with the experimentally observed time constant of ~10 ns for the triplet decay.<sup>20</sup> The different result between our calculations for the dinucleotide TpT and CASPT2 for TT pair<sup>19</sup> might be due to the different model systems used, and TpT should be closer to the natural situation of DNA strand.

Furthermore, the decay rate of the biradical intermediate (~60 ns)<sup>20</sup> can be explained. It can be seen in Figure 5 that the decay of the triplet biradical via ISC2 may lead to either the recovery to the ground-state reactant RS with a low barrier of 0.5 kcal mol<sup>-1</sup> or the formation of the CPD product with a barrier of 3.4 kcal mol<sup>-1</sup>. In either case, the spin multiplicity is altered from triplet to singlet. Also, along the PES in either the triplet or singlet ground state, the biradical intermediate at ISC2 is trapped in a local energy minimum. These two factors thus account for the observed long lifetime of the biradical intermediate (~60 ns).

Prior to reaching ISC2, another new T<sub>1</sub>/S<sub>0</sub> crossing point ISC1 has also been located in our calculations. The minimum energy path for ISC1 in the ground state (denoted with purple solid line in Figure 5) shows the relaxation back to the reactant. This adds a new physical quenching pathway for the triplet decay. This triplet quenching process via ISC1 is also rate-limited by the energy barrier of 12.9 kcal mol<sup>-1</sup> for reaching ISC1 from the triplet RT, consistent with the triplet decay time constant of ~10 ns.<sup>20</sup> The subsequent decay of ISC1 to ground-state reactant also requires spin flipping and should have time constant of ~60 ns, as for ISC2.

For the two T<sub>1</sub>/S<sub>0</sub> crossing points ISC1 and ISC2 that can lead to physical quenching, the spin-orbit coupling (SOC) constants were calculated. DFT calculations for spin-orbit coupling constants can be performed with DALTON program package<sup>38</sup> using the effective single-electron approximation<sup>39,40</sup> in linear response theory. The  $\omega$ B97XD functional is not available in DALTON program. The spin-orbit coupling matrix elements were therefore computed at the level of

B3LYP/6-311G(d,p) using the Breit–Pauli (BP) operator.<sup>41,42</sup> The SOC values of ISC1 and ISC2 are 4.37 and 1.08 cm<sup>-1</sup>, separately, as shown in Table 4. Except for SOC values,

**Table 4.** B3LYP/6-311G(d,p) Calculated Spin–Orbit Coupling Constant (cm<sup>-1</sup>) and the Singlet–Triplet Energy Gap (kcal mol<sup>-1</sup>) for ISC1 and ISC2

	$\langle\Psi_1 \hat{H}_x^{\text{BP}} \Psi_2\rangle$	$\langle\Psi_1 \hat{H}_y^{\text{BP}} \Psi_2\rangle$	$\langle\Psi_1 \hat{H}_z^{\text{BP}} \Psi_2\rangle$	SOC <sup>a</sup>	$\Delta E_{\text{S-T}}$
ISC1	-1.03	-2.88	-3.12	4.37	0.28
ISC2	-0.64	-0.10	0.87	1.08	0.57

<sup>a</sup>The square root of the sum of the three components' squares.

intersystem crossing probability is also dependent on energy gap between two states. Based on the energy gap law,<sup>43,44</sup> the quenching rate from one electronic state to another state increases exponentially with the decrease of the energy gap between the states.<sup>45,46</sup> As shown in Table 4, the singlet–triplet energy gaps for ISC1 and ISC2 are very small (0.28 and 0.57 kcal mol<sup>-1</sup>). The nearly degeneracy between the triplet and singlet state at the crossing point can guarantee the efficient intersystem crossing even with small spin–orbit coupling.<sup>31–34</sup> Therefore, intersystem crossing via either ISC1 or ISC2 constitute two efficient physical quenching pathways along the dimerization coordinate. This theoretical result supports the experimental observation that the biradical intermediate has a low propensity to form CPD but is mainly subject to a nonreactive decay.<sup>20</sup>

The third crossing point ISC3 is located after the triplet biradical intermediate (IM). For ISC3, the minimum energy path calculation shows that it leads to the formation of CPD in the ground state (denoted with orange solid line in Figure 5). A structure similar to ISC3 was located for two stacked thymines by using B3LYP hybrid density functional.<sup>18</sup> However, an energy barrier of approximately 16.7 kcal mol<sup>-1</sup> is required to reach ISC3 from the biradical intermediate IM. This makes it energetically less favorable as a pathway to form CPD, if compared with the pathway via ISC2 that is highlighted with red dotted lines in Figure 5. The nonadiabatic pathway forming CPD via ISC2 is only rate-limited by the barrier of 12.9 kcal mol<sup>-1</sup> for the triplet RT to TS1 and should take place easily at room temperature. However, ISC1 and ISC2, resulting in the S<sub>0</sub>-state recovery, also locate along the pathway to form CPD and could bring on a net result of physical quenching instead of CPD formation. This is consistent with the experiment results that the formation of CPD through triplet route is inefficient (less than 10%),<sup>8</sup> although the T<sub>1</sub> quenching rate constant is observed to be large (~10<sup>10</sup> M<sup>-1</sup> s<sup>-1</sup>).<sup>10,17</sup> Altogether, the theoretical results suggest that the self-quenching reaction pathways resulting in S<sub>0</sub> recovery should dominate and only a small fraction of triplet populations collapse into the photochemical CPD product.

## CONCLUSION

In summary, the present study has characterized the photochemical and photophysical evolution for the photoexcited dinucleotide TpT using DFT method. The potential energy profiles for the CPD formation in the S<sub>0</sub> and T<sub>1</sub> states as well as the interaction between these states are explored using the  $\omega$ B97XD/6-311G(d,p) level of theory. Compared with B3LYP functional,  $\omega$ B97XD functional with dispersion correction has improved the theoretical description of the formation of CPD.

The excitation energies for  $S_1(^1n\pi^*)$ ,  $T_4$ ,  $T_3$ ,  $T_2$ , and  $T_1$  are calculated at the TD- $\omega$ B97XD/6-311G(d,p) level of theory.

The calculated results indicate that following the initial excitation to the  $^1\pi\pi^*$  state, the underlying dark state  $^1n\pi^*$  governs the partitioning of the excited-state population between the two photophysical relaxation channels for the prevailing IC to  $S_0$  and the small intersystem crossing (ISC) conversion that results in a long-lived triplet state. It is shown that the triplet excited state  $T_4(^3\pi\pi^*)$  has negligible energy gap with  $^1n\pi^*$  state, resulting in a depopulation pathway of ISC to the triplet manifold followed by conversion via IC to the lowest  $T_1$  state, the long-lived reactive precursor to the photoproduct CPD.

The detailed examination for the  $T_1$  pathway reveals also the predominant photophysical quenching over the photochemical CPD formation. For the CPD formation via  $T_1$  mechanism, the most energetically feasible pathway corresponds to the first formation of the of a triplet biradical intermediate IM overcoming a barrier of 12.9 kcal mol<sup>-1</sup>, where the energy degeneracy between  $T_1$  and  $S_0$  occurs and results in the  $T_1/S_0$  surface crossing point ISC2. Via ISC2, the system crosses over to  $S_0$  state and completes the cross-linking to end product CPD. On the other hand, the existence of ISC2 could also lead to a deactivation pathway, from which the biradical intermediate is reverted back to the ground-state reactant nearly barrierlessly. In addition to ISC2, another new  $T_1/S_0$  crossing point ISC1 exists prior to the triplet biradical intermediate IM. Through ISC1, the triplet reactant can decay back to the  $S_0$  state, without even undergoing further CPD cross-linking. The two deactivation pathways via  $T_1/S_0$  surface crossing points guarantee that most of the triplets undergo reversion back into the ground-state reactant, whereas only a small fraction is transformed to photoproduct CPD. These results explain the experimental observation that the  $T_1$  quenching, though efficient, gives only a very low quantum yield of the photoproduct CPD.<sup>8</sup> Meanwhile, our calculations reveal that a barrier of 12.9 kcal mol<sup>-1</sup> is required for the decay of the locally excited triplet state to the biradical intermediate, providing rationale for the most recent experimental observation that triplet decay in (dT)<sub>18</sub> or the locked dinucleotide T<sub>1</sub>pT<sub>1</sub> follows nanosecond rates (~10 ns).<sup>20</sup> Overall, the finding of physical quenching pathways in competition with CPD formation allow for a deeper understanding of the inefficiency of deleterious CPD formation and ultimately shed light on DNA photostability.

## AUTHOR INFORMATION

### Corresponding Author

\*H. Su: Tel: +86-10-62562837. E-mail: hongmei@iccas.ac.cn.

### Notes

The authors declare no competing financial interest.

## ACKNOWLEDGMENTS

This work was financially supported by the National Natural Science Foundation of China (Grant No. 21203206, 21333012), the National Basic Research Program of China (2013CB834602), and the Chinese Academy of Sciences (project XDB12020200). The calculations were supported by the Supercomputing Center, Computer Network Information Center of Chinese Academy of Sciences. Thanks to Di Fan in the Institute of Chemistry for helpful discussion.

## REFERENCES

- (1) Sinha, R. P.; Hader, D. P. UV-induced DNA Damage and Repair: A Review. *Photochem. Photobiol. Sci.* **2002**, *1*, 225–236.
- (2) Du, Q.; Zhao, H.; Song, D.; Liu, K.; Su, H. Consecutive Reaction Mechanism for the Formation of Spore Photoproduct in DNA Photolesion. *J. Phys. Chem. B* **2012**, *116*, 11117–11123.
- (3) Clingen, P. H.; Arlett, C. F.; Roza, L.; Mori, T.; Nikaido, O.; Green, M. H. L. Induction of Cyclobutane Pyrimidine Dimers, Pyrimidine(6–4)pyrimidone Photoproducts, and Dewar Valence Isomers by Natural Sunlight in Normal Human Mononuclear Cells. *Cancer Res.* **1995**, *55*, 2245–2248.
- (4) Mouret, S.; Baudouin, C.; Charveron, M.; Favier, A.; Cadet, J.; Douki, T. Cyclobutane Pyrimidine Dimers are Predominant DNA Lesions in Whole Human Skin Exposed to UVA Radiation. *Proc. Natl. Acad. Sci. U. S. A.* **2006**, *103*, 13765–13770.
- (5) Schreier, W. J.; Schrader, T. E.; Koller, F. O.; Gilch, P.; Crespo-Hernandez, C. E.; Swaminathan, V. N.; Carell, T.; Zinth, W.; Kohler, B. Thymine Dimerization in DNA is an Ultrafast Photoreaction. *Science* **2007**, *315*, 625–629.
- (6) Boggio-Pasqua, M.; Groenhof, G.; Schäfer, L. V.; Grubmüller, H.; Robb, M. A. Ultrafast Deactivation Channel for Thymine Dimerization. *J. Am. Chem. Soc.* **2007**, *129*, 10996–10997.
- (7) McCullagh, M.; Hariharan, M.; Lewis, F. D.; Markovitsi, D.; Douki, T.; Schatz, G. C. Conformational Control of TT Dimerization in DNA Conjugates. A Molecular Dynamics Study. *J. Phys. Chem. B* **2010**, *114*, 5215–5221.
- (8) Banyasz, A.; Douki, T.; Improta, R.; Gustavsson, T.; Onidas, D.; Vayá, I.; Perron, M.; Markovitsi, D. Electronic Excited States Responsible for Dimer Formation upon UV Absorption Directly by Thymine Strands: Joint Experimental and Theoretical Study. *J. Am. Chem. Soc.* **2012**, *134*, 14834–14845.
- (9) Marguet, S.; Markovitsi, D. Time-resolved Study of Thymine Dimer Formation. *J. Am. Chem. Soc.* **2005**, *127*, 5780–5781.
- (10) Kwok, W. M.; Ma, C.; Phillips, D. L. A Doorway State Leads to Photostability or Triplet Photodamage in Thymine DNA. *J. Am. Chem. Soc.* **2008**, *130*, 5131–5139.
- (11) Mills, J. B.; Vacano, E.; Hagerman, P. J. Flexibility of Single-stranded DNA: Use of Gapped Duplex Helices to Determine the Persistence Lengths of Poly(dT) and Poly(dA). *J. Mol. Biol.* **1999**, *285*, 245–257.
- (12) Douki, T.; Court, M.; Sauvaigo, S.; Odin, F.; Cadet, J. Formation of the Main UV-induced Thymine Dimeric Lesions within Isolated and Cellular DNA as Measured by High Performance Liquid Chromatography-tandem Mass Spectrometry. *J. Biol. Chem.* **2000**, *275*, 11678–11685.
- (13) Moysan, A.; Viari, A.; Vigny, P.; Voituriez, L.; Cadet, J.; Moustacchi, E.; Sage, E. Formation of Cyclobutane Thymine Dimers Photosensitized by Pyridopsoralens: Quantitative and Qualitative Distribution within DNA. *Biochemistry* **1991**, *30*, 7080–7088.
- (14) Nikogosyan, D. N. Two-quantum UV Photochemistry of Nucleic Acids: Comparison with Conventional Low-intensity UV Photochemistry and Radiation Chemistry. *Int. J. Radiat. Biol.* **1990**, *57*, 233–299.
- (15) Görner, H. Photochemistry of DNA and Related Biomolecules: Quantum Yields and Consequences of Photoionization. *J. Photochem. Photobiol. B: Biol.* **1994**, *26*, 117–139.
- (16) Görner, H. Transients of Uracil and Thymine Derivatives and the Quantum Yields of Electron Ejection and Intersystem Crossing upon 20 ns Photolysis at 248 nm. *Photochem. Photobiol.* **1990**, *52*, 935–948.
- (17) Yang, C.; Yu, Y.; Liu, K.; Song, D.; Wu, L.; Su, H. [2 + 2] Photocycloaddition Reaction Dynamics of Triplet Pyrimidines. *J. Phys. Chem. A* **2011**, *115*, 5335–5345.
- (18) Zhang, R. B.; Eriksson, L. A. A Triplet Mechanism for the Formation of Cyclobutane Pyrimidine Dimers in UV-Irradiated DNA. *J. Phys. Chem. B* **2006**, *110*, 7556–7562.
- (19) Climent, T.; Gonzalez-Ramirez, I.; Gonzalez-Luque, R.; Merchan, M.; Serrano-Andres, L. Cyclobutane Pyrimidine Photo-

dimerization of DNA/RNA Nucleobases in the Triplet State. *J. Phys. Chem. Lett.* **2010**, *1*, 2072–2076.

(20) Pilles, B. M.; Bucher, D. B.; Liu, L.; Clivio, P.; Gilch, P.; Zinth, W.; Schreier, W. J. Mechanism of the Decay of Thymine Triplets in DNA Single Strands. *J. Phys. Chem. Lett.* **2014**, *5*, 1616–1622.

(21) Chai, J.-D.; Head-Gordon, M. Long-range Corrected Hybrid Density Functionals with Damped Atom-atom Dispersion Corrections. *Phys. Chem. Chem. Phys.* **2008**, *10*, 6615–6620.

(22) Céline, D.; Chandan, P.; Elise, D. Improved DFT Description of Intrastrand Cross-Link Formation by Inclusion of London Dispersion Corrections. *J. Phys. Chem. B* **2011**, *115*, 15138–15144.

(23) Gonzalez, C.; Schlegel, H. B. Reaction Path Following in Mass-Weighted Internal Coordinates. *J. Phys. Chem.* **1990**, *94*, 5523–5527.

(24) Mennucci, B.; Tomasi, J. Continuum Solvation Models: A New Approach to the Problem of Solute's Charge Distribution and Cavity Boundaries. *J. Chem. Phys.* **1997**, *106*, 5151–5158.

(25) Durbeej, B.; Eriksson, L. A. Reaction Mechanism of Thymine Dimer Formation in DNA Induced by UV Light. *J. Photochem. Photobiol.* **2002**, *152*, 95–101.

(26) Becke, A. D. Density-functional Thermochemistry. III. The Role of Exact Exchange. *J. Chem. Phys.* **1993**, *98*, 5648–5652.

(27) Lee, C. T.; Yang, W. T.; Parr, R. G. Development of the Colle-Salvetti Correlation-Energy Formula into a Functional of the Electron Density. *Phys. Rev. B* **1988**, *37*, 785–789.

(28) Frisch, M. J.; Trucks, G. W.; Schlegel, H. B.; Scuseria, G. E.; Robb, M. A.; Cheeseman, J. R.; Scalmani, G.; Barone, V.; Mennucci, B.; Petersson, G. A.; et al. *Gaussian 09*, Revision D.01; Gaussian, Inc.: Wallingford, CT, 2009.

(29) Serrano-Pérez, J. J.; González-Luque, R.; Merchán, M.; Serrano-Andrés, L. On the Intrinsic Population of the Lowest Triplet State of Thymine. *J. Phys. Chem. B* **2007**, *111*, 11880–11883.

(30) Turro, N. J. *Modern Molecular Photochemistry*; University Science. Book: Mill Valley, CA, 1991.

(31) Parker, D. S. N.; Minns, R. S.; Penfold, T. J.; Worth, G. A.; Fielding, H. H. Ultrafast Dynamics of the S<sub>1</sub> Excited State of Benzene. *Chem. Phys. Lett.* **2009**, *469*, 43–47.

(32) Penfold, T. J.; Worth, G. A. The Effect of Molecular Distortions on Spin-orbit Coupling in Simple Hydrocarbons. *Chem. Phys.* **2010**, *375*, 58–66.

(33) Marian, C. M. Spin-Orbit Coupling and Intersystem Crossing in Molecules. *WIREs. Comput. Mol. Sci.* **2012**, *2*, 187–203.

(34) Richter, M.; Marquetand, P.; González-Vázquez, J.; Sola, I.; González, L. Femtosecond Intersystem Crossing in the DNA Nucleobase Cytosine. *J. Phys. Chem. Lett.* **2012**, *3*, 3090–3095.

(35) Etinski, M.; Fleig, T.; Marian, C. Intersystem Crossing and Characterization of Dark States in the Pyrimidine Nucleobases Uracil, Thymine, and 1-methylthymine. *J. Phys. Chem. A* **2009**, *113*, 11809–11816.

(36) Hare, P. M.; Crespo-Hernández, C. E.; Kohler, B. Internal Conversion to the Electronic Ground State Occurs via Two Distinct Pathways for Pyrimidine Bases in Aqueous Solution. *Proc. Natl. Acad. Sci. U. S. A.* **2007**, *104*, 435–440.

(37) Hare, P. M.; Crespo-Hernández, C. E.; Kohler, B. Solvent-dependent Photophysics of 1-cyclohexyluracil: Ultrafast Branching in the Initial Bright State Leads Nonradiatively to the Electronic Ground State and a Long-lived <sup>1</sup>nπ\* State. *J. Phys. Chem. B* **2006**, *110*, 18641–18650.

(38) Helgaker, T.; Jensen, H. J. A.; Jørgensen, P.; Olsen, J.; Ruud, K.; Ågren, H.; Bak, K. L.; Bakken, V.; Christiansen, O.; Dahle, P.; et al. An ab initio electronic structure program, Release 1.1 (July 2000). See <http://www.kjemi.uio.no/software/dalton/dalton.html>.

(39) Koseki, S.; Fedorov, D. G.; Schmidt, M. W.; Gordon, M. S. Spin-Orbit Splittings in the Third-Row Transition Elements: Comparison of Effective Nuclear Charge and Full Breit-Pauli Calculations. *J. Phys. Chem. A* **2001**, *105*, 8262–8268.

(40) Koseki, S.; Schmidt, M. W.; Gordon, M. S. Effective Nuclear Charges for the First- through Third-Row Transition Metal Elements in Spin-Orbit Calculations. *J. Phys. Chem. A* **1998**, *102*, 10430–10435.

(41) Nicklass, A.; Peterson, K. A.; Berning, A.; Werner, H.; Knowles, P. J. Convergence of Breit-Pauli Spin-Orbit Matrix Elements with Basis Set Size and Configuration Interaction Space: The Halogen Atoms F, Cl, and Br. *J. Chem. Phys.* **2000**, *112*, 5624–5632.

(42) Berning, A.; Schweizer, M.; Werner, H.; Knowles, P. J.; Palmieri, P. Spin-orbit Matrixelements for Internally Contracted Multireference Configuration Interaction Wavefunctions. *Mol. Phys.* **2000**, *98*, 1823–1833.

(43) Englman, R.; Jortner, J. The Energy Gap Law for Radiationless Transitions in Large Molecules. *J. Mol. Phys.* **1970**, *18*, 145–164.

(44) Lin, S. H. The Energy Gap Law and Franck-Condon Factor in Radiationless Transitions. *J. Chem. Phys.* **1970**, *53*, 3766–3767.

(45) Peng, Q.; Niu, Y. L.; Shi, Q. H.; Gao, X.; Shuai, Z. G. Correlation Function Formalism for Triplet Excited State Decay: Combined Spin – Orbit and Nonadiabatic Couplings. *J. Chem. Theory Comput.* **2012**, *9*, 1132–1143.

(46) Niu, Y. L.; Peng, Q.; Deng, C. M.; Gao, X.; Shuai, Z. G. Theory of Excited State Decays and Optical Spectra: Application to Polyatomic Molecules. *J. Phys. Chem. A* **2010**, *114*, 7817–7831.